Langmuir

Article

pubs.acs.org/Langmuir

Alcohol Dispersions of Calcium Hydroxide Nanoparticles for Stone Conservation

Carlos Rodriguez-Navarro,* Amelia Suzuki, and Encarnacion Ruiz-Agudo

Department of Mineralogy and Petrology, University of Granada, Fuentenueva s/n, 18002 Granada, Spain

ABSTRACT: Alcohol dispersions of $Ca(OH)_2$ nanoparticles, the so-called *nanolimes*, are emerging as an effective conservation material for the consolidation of stone, mortars, and plasters present in old masonry and/or mural paintings. To better understand how this treatment operates, to optimize its performance and broaden its applications, here we study the nano and microstructural characteristics, carbonation behavior, and consolidation efficacy of colloidal alcohol dispersions of $Ca(OH)_2$ nanoparticles produced by both homogeneous (commercial nanolime) and heterogeneous phase synthesis (aged slaked lime and carbide lime putties). We observe that the alcohol not only provides a high colloidal stability to $Ca(OH)_2$ particles, but also affects the kinetics of carbonation and $CaCO_3$ polymorph selection. This is due to the pseudomorphic replacement of $Ca(OH)_2$ particles by calcium alkoxides upon reaction with ethanol or 2-propanol. The extent of this replacement reaction depends on $Ca(OH)_2$ size and time. Hydrolysis of alkoxides speeds up the carbonation process and increases the $CaCO_3$ yield. The higher degree of transformation into calcium alkoxide of both the commercial nanolime and the carbide lime fosters metastable vaterite formation, while calcite precipitation is promoted upon carbonation of the aged slaked lime due its lower reactivity, which limits calcium alkoxide formation. A higher consolidation efficacy in terms of strength gain of treated porous stone is achieved in the latter case, despite the fact that the carbonation is much faster and reaches a higher yield in the former ones. Formation of alkoxides, which has been neglected in previous studies, needs to be considered when applying nanolime treatments. These results show that the use $Ca(OH)_2$ nanoparticle dispersions prepared with either aged slaked lime or carbide lime putties is an economical and effective conservation alternative to commercial nanolimes produced by homogeneous phase synthesis. Ultimately, this study contributes to show that nanotechnology can help saving the built and sculptural heritage.

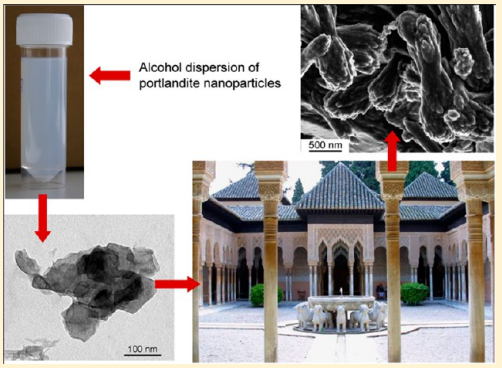

1. INTRODUCTION

The survival of mankind's cultural heritage is challenged by chemical, physical, and biological weathering phenomena.[1] In an attempt to halt and/or mitigate the degradation of materials used in the built and sculptural heritage, several conservation treatments have been developed and applied.[1] Until recently, most widely used treatments for the protection and consolidation of damaged stone, mortars and plasters, and mural paintings involved the application of synthetic polymers such as acrylic, epoxy, or (poly)vinyl resins, as well as their copolymers. However, polymer protectives and consolidants are generally incompatible (physically and chemically) with the inorganic substrate they are applied to, thus fostering damage.[3] For instance, Giorgi et al.[3] report on the deleterious effects of a copolymer treatment (vinyl-acetate/*n*-butyl-acrylate) applied on degraded mural paintings in the Maya site of Mayapan (Yucatan, Mexico). The formation of an impervious organic surface coating led to enhanced salt damage and the loss of painted areas.

The physicochemical incompatibility and poor aging of most polymer-based conservation treatments have prompted the resurgence of inorganic conservation materials.[4] One of their principal advantages is that they can be chemically and structurally similar to the inorganic substrate they are applied to, thereby ensuring a high compatibility. There is a long tradition on the use of inorganic compounds for the protection and consolidation of building materials such as stone. For instance, limewater, i.e., a calcium hydroxide saturated solution, has been applied to consolidate degraded porous substrates, especially those of carbonatic nature (e.g., limestones or lime mortars).[4] During carbonation, atmospheric CO_2 dissolves in the calcium hydroxide solution, leading to precipitation of calcium carbonate according to the (overall) reaction: $Ca(OH)_2 + CO_2 = CaCO_3 + H_2O$. The newly formed $CaCO_3$ can act as a cement, binding loose grains and/or filling cracks. However, the limewater method does not seem to be very effective,[1,4] principally because of the limited solubility of $Ca(OH)_2$ in water (1.7 g L^{-1} at 20 °C) which precludes the introduction of sufficient amounts of consolidant into the porous system of the treated material.[5] The use of large quantities of water is also an important risk:[6] e.g., potential substrate dissolution, clay-swelling, mobilization of salts (fostering salt weathering), or freeze−thaw damage.

Received: May 9, 2013
Revised: July 1, 2013
Published: August 6, 2013

 © 2013 American Chemical Society dx.doi.org/10.1021/la4017728 | *Langmuir* 2013, 29, 11457−11470

To overcome the limitations of the limewater treatment, Giorgi et al.[5] proposed the use of aliphatic alcohol dispersions of portlandite ($Ca(OH)_2$) particles for the protection and consolidation of limestone and, particularly, lime-based plasters with painted surfaces. The authors reported that aqueous suspensions of portlandite particles were kinetically unstable and settled rapidly. In addition, the higher contact angle and viscosity of water, and the resulting limited sorptivity,[7] precluded a sufficiently high penetration of the suspended particles once applied on a porous substrate. These effects resulted in unacceptable surface white glazing. By using short-chain alcohols (e.g., 1-propanol), Giorgi et al.[5] obtained highly stable dispersions of $Ca(OH)_2$ particles which enabled the consolidation of lime mortars and mural paintings. In this pioneering study, $Ca(OH)_2$ dispersions were prepared using dry hydrated lime (powder) or slaked lime (lime putty) (i.e., produced via heterogeneous synthesis, see below) with micrometer-sized particles, presumably aggregates of submicrometer primary particles. Afterward, colloidal $Ca(OH)_2$ nanoparticles were homogeneously synthesized in diols,[8] aqueous solutions,[9] and water-in-oil microemulsions.[10] This bottom-up synthesis resulted in nanophase portlandite crystals, known as nanolimes. It was reported that nanolimes have superior properties, including a higher reactivity, a higher penetration efficiency, and a higher kinetic stability when dispersed in aliphatic alcohols such as ethanol, 1-propanol, or 2-propanol.[11,12] Recent studies have focused on the analysis of the carbonation, consolidation efficacy, and improvement in the homogeneous synthesis of nanolimes applied to the consolidation of stone, lime mortars, and mural painting, as well as for paper, canvas, and wood deacidification.[2,12−14]

Currently, the standard route for the preparation of nanolimes is homogeneous phase synthesis in an aqueous solution. However, this route has some drawbacks.[14] First, the synthesis has to be performed at $T \geq 90$ °C and is time-consuming as it involves the dropwise addition of NaOH solution to an aqueous solution of $CaCl_2$,[15] or $Ca(NO_3)_2$,[16] under vigorous stirring. Second, the resulting NaCl (or $NaNO_3$) byproduct has to be eliminated. For this task, after discarding the supernatant, the remaining suspension is washed with deionized water up to 5 times.[9] Finally, the aqueous dispersion of portlandite particles is dispersed in alcohol (typically, ethanol or 2-propanol) at a desired concentration (e.g., 5 g/L). All in all, this synthesis route is costly and the yield is low. But there is an additional problem: during each washing/rinsing performed to eliminate residual Na salt, a fraction of $Ca(OH)_2$ particles will be dissolved. Of all $Ca(OH)_2$ particles, those with size <100 nm would be preferentially dissolved, as they are more soluble. The claimed advantage of homogeneous synthesis as a way to obtain $Ca(OH)_2$ nanoparticles (i.e., with average size ≤100 nm) is thus challenged. This may explain why the particle size of nanolimes produced by homogeneous phase synthesis ranges between 100 and 300 nm.[11,13,15] These limitations could be partially overcome by homogeneous phase synthesis in the presence of additives (e.g., ethylene glycol), followed by repeated rinsing of the precipitates with saturated $Ca(OH)_2$ solution and elimination of excess solution via dialysis.[17] However, this latter process is also time-consuming: just the dialysis takes 3 days.

$Ca(OH)_2$ nanoparticles can also be obtained via heterogeneous phase synthesis.[3,18,19] Heterogeneous synthesis of $Ca(OH)_2$ is readily achieved upon hydration (or slaking) of lime (CaO) produced by calcination of $CaCO_3$.[20] Several parameters affect the slaking process and the properties of the resulting hydroxide crystals, such as CaO reactivity, oxide/water ratio, slaking water T, local overheating, vapor- vs liquid-phase hydration, and presence of additives (e.g., alcohols).[18,19] In addition, aging of slaked lime putty leads to a reduction of portlandite crystals size and the overdevelopment of (0001) basal faces. These nanoparticles have a high surface/volume ratio, which enhances their reactivity (e.g., dissolution kinetics and carbonation rate), and their dispersions show a high colloidal stability and improved rheological properties.[19,20] Slaked lime is typically made up of primary $Ca(OH)_2$ nanoparticles 20 to 300 nm in size.[18,19] Aggregation leads to significant size polydispersity due to the formation of micrometer-sized clusters. Our previous studies suggest that the high yield, ease of preparation, and nanosized nature of aged slaked lime putty make it a good candidate for stone consolidation using the nanolime methodology developed by Baglioni's group.[5]

Heterogeneous synthesis of portlandite nanoparticles also takes place during several industrial processes, including paper and acetylene (C_2H_2) production. In the latter case, the so-called carbide lime or lime sludge is produced.[21,22] Carbide lime (CL) forms as a byproduct of the hydrolysis of Ca_2C in water leading to the generation of C_2H_2 and CaO. The newly formed CaO rapidly hydrates, yielding a $Ca(OH)_2$ slurry. CL is an impure hydroxide which contains residues of both inorganic carbon (unreacted carbon) and organic carbon (hydrocarbons), along with traces of sulfur compounds (H_2S) and aluminosilicates.[21,22] CL may also include trace amounts of metals such as Fe, Pb, Cu, Cd, Ni, Cd, and Zn.[22] These residues originate from impurities present in the coal and limestone used for calcium carbide synthesis, which takes place at a high T (2300 °C) according to the reaction $CaO + 3C = CaC_2 + CO$ ($CO + 1/2O_2 = CO_2$). Although CL has found some applications in the cement industry, soil stabilization, agriculture, asphaltic paving mixes, and sewage/water treatment,[21,22] the presence of impurities has precluded/limited the use of this waste material for the numerous industrial and technical applications of $Ca(OH)_2$.[21,22] In fact, this waste lime is typically discarded and accumulated in ponds.[22] This procedure is an economical burden and possesses some environmental risks (e.g., accidental spilling and/or groundwater contamination).

We have recently patented a purification process for CL involving the oxidation of the organic carbon and sulfur compounds, the precipitation of the latter as insoluble barite ($BaSO_4$) following addition of $Ba(OH)_2$, and immobilization (coprecipitation) of heavy metals in the insoluble barite which is subsequently eliminated by gravity separation.[22] This purified material, with commercial name Geosilex, is an aqueous dispersion of $Ca(OH)_2$ nanoparticles (carbide lime putty) which typically includes a dispersant such as lignosulfonate (0.001−0.01 wt %), added to avoid bleeding and to foster disaggregation of $Ca(OH)_2$ particles. Its physicochemical characteristics are very similar to those of aged slaked lime putty. In addition to its nanophase nature, the purified CL has the principal advantage of being a waste product whose recycling is environmentally friendly and of economic significance. Currently, this purified CL is finding applications in the construction industry as a binder with a net positive CO_2-capture balance. Due to its nanophase character, carbide lime putty should also be a good alternative for the preparation of nanolime dispersions for conservation applications.

dx.doi.org/10.1021/la4017728 | Langmuir 2013, 29, 11457−11470

It is our aim to explore here the potential of $Ca(OH)_2$ nanoparticles in aged slaked lime and carbide lime putties as an economic and effective alternative to nanolimes produced by homogeneous phase synthesis for the conservation of stone. For this task we first characterize the compositional and microstructural features of these two lime putties and compare them with those of a commercial nanolime (Nanorestore). Then, we study their kinetic stability in alcohol dispersions and their carbonation behavior. We pay special attention to the study of $Ca(OH)_2$-alcohol interaction (i.e., formation of calcium alkoxides) and its effect on $CaCO_3$ polymorph selection and carbonation kinetics. This is an important aspect that has been neglected in previous works. Finally, we test the consolidation efficiency of alcohol dispersions of aged slaked lime, carbide lime, and commercial nanolime $Ca(OH)_2$ nanoparticles applied to a porous building stone.

2. MATERIALS AND METHODS

2.1. Lime Putties. Two types of lime putty were used. One was a traditional aged slaked lime putty (FG) which was prepared via heterogeneous phase synthesis.[19] CaO pebbles, ca. 1−2 cm in size, were slaked in deionized water under vigorous stirring. The water/oxide weight ratio was 1:4, yielding a slaked lime putty with a typical solid volume fraction, ϕ, of ∼0.23. The resulting paste was stored in an airtight plastic container for 5 years aging time prior to its use. The other type of $Ca(OH)_2$ was a carbide lime paste (CL) supplied by Trenzametal S.L. (Zamora, Spain). This CL paste was subjected to a patented purification process.[22] The paste had a light-gray color (due to the presence of graphite traces; see below) and ϕ of ∼0.15. Care was taken to avoid early carbonation of the lime putties during processing and storage (they were kept in airtight plastic containers).

2.2. Alcohol Dispersions and Kinetic Stability Measurements. Ethanol (Panreac, puriss.) and 2-propanol (Panreac, puriss.) dispersions of $Ca(OH)_2$ were prepared using FG and CL lime putties. The solid content was 5 g/L, as it is commonly suggested in the nanolime literature.[11] The alcohol dispersions included ca. 1 wt % residual water (i.e., originally present in the lime putties). Equal solid content aqueous dispersions of $Ca(OH)_2$ particles were prepared as controls.

We also used a commercial nanolime (NL) sold under the trade name Nanorestore (CTS, Italy). This is a 2-propanol dispersion of $Ca(OH)_2$ nanoparticles (5 g/L solid concentration) produced by homogeneous phase synthesis in an aqueous solution. This type of commercial nanolime has been extensively used for conservation purposes.[12,23]

The relative kinetic stability of the dispersions was calculated from the variation over time of the ratio of the optical density of the supernatant liquid and of the original dispersion determined at 600 nm (UV−vis spectrophotometer, Thermo Spectronic UNICAM UV 300).[3] Right before analysis, the dispersions were subjected to 5 min ultrasonic bath (Ultrasons model, 200 W; J. P. Selecta), and introduced in standard plastic cuvettes (10 mm optical path). Cuvettes were not capped during measurements in order to evaluate the evolution of the kinetic stability of dispersions following air-exposure (i.e., partial carbonation) as occurs during real application conditions (e.g., impregnation, brushing or spraying on a stone surface).

2.3. Analysis of $Ca(OH)_2$ Particles. Mineralogy and crystallite size/strain of the solids in FG and CL putties as well as in the commercial nanolime (NL) were determined by X-ray diffraction (XRD) on a Philips PW-1710 diffractometer equipped with an automatic slit or on a XPert Philips with Ni filter. Measurement parameters: Cu Kα radiation λ = 1.5405 Å, 45 kV, 40 mA, 4 to 70° 2θ exploration range, steps of 0.001° 2θ, and goniometer speed of 0.01° 2θ s^{-1}. Powders obtained upon drying at room T under flowing N_2 and drying in an air-ventilated oven (95 °C, 24 h) were deposited in zero-background Si sample holders. Mineral phases were identified by comparison with JCPDS powder spectra (Joint Committee on Powder Diffraction Standards). No differences in mineral composition/content (and FTIR spectral features; see below) associated with the drying conditions were observed; this is why data reported here (unless indicated) correspond to oven-dried samples (i.e., easier sample preparation). Peak broadening analysis enabled the determination of crystallite size, D_{hkl}, (i.e., coherent X-ray scattering domains) and lattice strain, ε of $Ca(OH)_2$ crystals.[24] For this task, the Williamson-Hall method was used.[25] XRD data collection and peak broadening analysis were performed using the XPowder 1.2 software package, which enables background subtraction, Kα_2 stripping, and instrumental broadening correction.[26] Peak profile fitting was performed using Gaussian, Lorentzian, and pseudo-Voigt functions. Best fits were obtained using a pseudo-Voight function (with Gaussian contribution <15%).

Additional compositional and microstructural features of $Ca(OH)_2$ particles were determined by means of field emission scanning electron microscopy (FESEM, Leo Gemini 1530), transmission electron microscopy (TEM, Philips CM20, 200 kV acceleration voltage), N_2 sorption at 77.3 K (Micromeritics TriStar 3000; samples were prepared by oven drying at 95 °C both aqueous putties and alcohol dispersions), micro-Raman spectroscopy (JASCO NRS-5100, equipped with a 532 nm diode laser), Fourier transform infrared spectroscopy (FTIR, Nicolet 20SXB with a resolution of 0.4 cm^{-1}; samples prepared by oven drying at 95 °C and/or drying at room T under flowing N_2; KBr pellets were used), and thermogravimetry (TG, Shimadzu TGA-50H equipped with a Delta microbalance; samples of ∼50 mg were placed in Al sample holders and analyzed in air or N_2, flowing at a rate of 120 mL/min, and at a heating rate of 20 °C/min). Further details on sample preparation and specific characteristics of the above listed analytical equipment have been published elsewhere.[18]

The particle size distribution (PSD) of portlandite suspensions (particles dispersed in ethanol and/or 2-propanol) was determined by laser scattering on a Malvern Hydro 2000 μp equipment. Note that this type of PSD analysis yields accurate information of aggregates but not necessarily of primary (nano)particles. For the size-analysis of primary particles, a higher accuracy is found using TEM.[19]

2.4. Carbonation of $Ca(OH)_2$ Particles. Both water and alcohol dispersions of FG and CL particles were deposited on glass slides and oven-dried at 95 °C for 60 min. In addition, samples were allowed to dry in air at room T. Although mineral phases formed after carbonation were similar in both cases, the latter drying method was ruled out as carbonation of the $Ca(OH)_2$ saturated solution was very fast during the initial drying period in the case water dispersions, thus precluding any meaningful comparison between the carbonation of water and alcohol dispersions. Once oven-dried, the samples were placed in a plastic container at 18 ± 2 °C and 80 ± 5% relative humidity (RH). The container was not airtight in order to allow a small but continuous flux of air ($pCO_2 \sim 10^{-3.5}$ atm) for carbonation to take place. A relatively high RH was selected in order to speed up the carbonation process. It is well-known that carbonation rates are strongly dependent on pH_2O. In particular, carbonation is sped up at RH ≥ 75% when multilayer adsorption of H_2O onto $Ca(OH)_2$ occurs.[27] To single out the possible role of lignosulfonate additive present in commercial CL on $CaCO_3$ polymorph selection (i.e., vaterite vs calcite), an additional carbonation test was performed using water and alcohol dispersions of additive-free CL. The carbonation of NL 2-propanol dispersion was also studied.

Samples were analyzed by XRD at predetermined time intervals (up to 60 days). The ratio (phase fraction) of calcite (C) to vaterite (V) in carbonated $Ca(OH)_2$ was calculated based on the relationship between the integral intensities (I_{hkl}) of the main Bragg peaks of each phase according to Rao's equation:[28]

$$X_C = \frac{I_{104C}}{I_{110V} + I_{112V} + I_{114V} + I_{104C}} \quad (1)$$

where X_C and the mass fraction of calcite (the mass fraction of vaterite, $X_V = 1 - X_C$). XRD results also enabled the study of carbonation kinetics. For this task, a calibration curve for semiquantitative XRD analysis was obtained. This was done by measuring the intensity ratio of portlandite (I_{101P}) to calcite (I_{104C}) main Bragg peaks in mixtures of

dx.doi.org/10.1021/la4017728 | Langmuir 2013, 29, 11457−11470

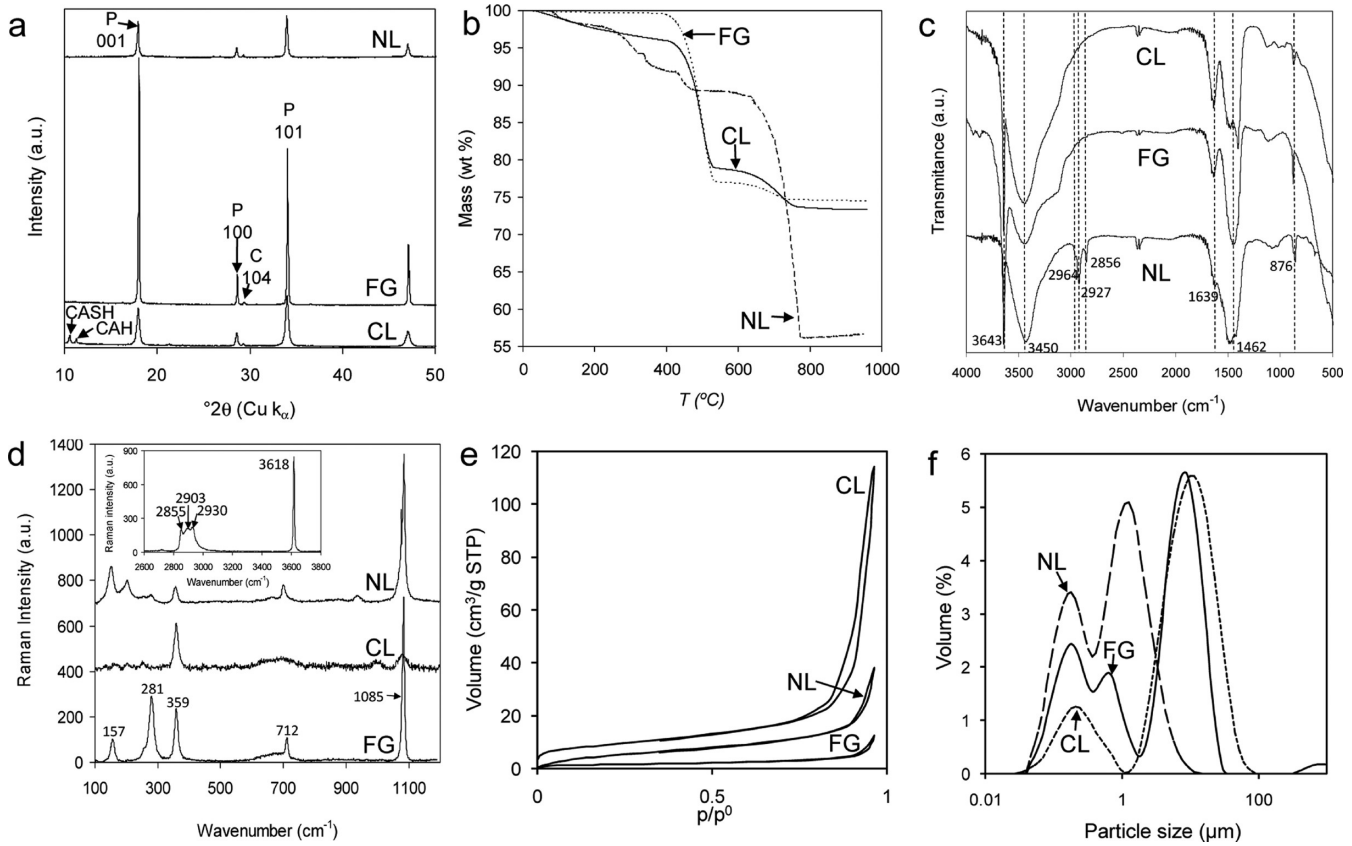

Figure 1. Characterization of FG, CL, and NL particles: (a) XRD patterns. Main Bragg peaks for portlandite (P), calcite (C), calcium aluminum silicate hydrate (CASH), and calcium aluminum hydroxide (CAH) are indicated; (b) TG traces; (c) FTIR spectra—wavenumbers of main bands are indicated; (d) micro-Raman spectra. Main Raman shifts are indicated. Inset shows a detail of the Raman spectra of the commercial nanolime (NL) at high wavenumbers (2600–3800 cm^{-1}); (e) N_2 sorption isotherms; and (f) particle size distribution (PSD).

both phases with X_C ranging from 0.1 to 0.9. Using this calibration curve, the actual concentration of calcite and portlandite was determined in samples subjected to carbonation for different periods of time. The calibration curve for calcite/portlandite mixtures was also used to study the carbonation rate of samples with vaterite, or mixtures of vaterite plus calcite. In these cases, and according to eq 1, the total I_{hkl} for the $CaCO_3$ mixture is $I_{104C} + I_{110V} + I_{112V} + I_{114V}$. Because the error associated to this type of (semiquantitative) XRD analysis is relatively high (ca. ± 5 wt %),[24] carbonation rates are considered appropriate to study differences among the studied samples, but are not intended to be purely quantitative.

2.5. Consolidation of Stone. Consolidation of a porous stone was performed using alcohol dispersions of FG and CL. Treatments were performed using ethanol dispersions because (i) kinetic stability measurements (see following section) showed that ethanol dispersions were more stable than 2-propanol dispersions, and (ii) recent studies have shown that nanolime dispersions in ethanol tend to produce better results than 2-propanol when applied as consolidants on different substrates.[6] For comparison purposes, we also performed consolidation tests using NL. Considering that past studies on the consolidation of stone using nanolime dispersions have focused on carbonate stones such as limestones, here we test the ability of these treatments to consolidate silicate stones. The stone selected for treatment was a sandstone from the Czech Republic, widely used in the city of Prague (e.g., Charles bridge). It is a poorly cemented quartzitic sandstone made up of subangular quartz (SiO_2) grains (average size ~200 μm), with minor amounts of K-feldspar ($KAlSiO_3$). It also includes kaolinite ($Al_2Si_2O_5(OH)_4$) as sparse intergranular cement. It has a high porosity (~29%) and a monodisperse pore size distribution with mean pore radius of ~10 μm, according to mercury intrusion porosimetry (MIP, Micromeritics Autopore 3000). These properties make this stone highly prone to deterioration. The siliceous nature of the stone and the lack of carbonate minerals facilitate the evaluation of the treatment penetration depth and the identification of the newly formed $CaCO_3$ cement. These features make this stone a good candidate to test the efficiency of the $Ca(OH)_2$ consolidation treatment.

Sandstone blocks 5 × 5 × 1 cm^3 in size were prepared and subjected to treatment with ethanol dispersions of FG and CL $Ca(OH)_2$ particles (5 g/L), as well as with 2-propanol NL dispersion (5 g/L). The treatment was applied by imbibition. This was performed by filling the bottom of crystallization dishes with the alcohol dispersions (up to 2 mm), which were sonicated for 5 min prior to use. Afterward, a stone block per crystallization dish was placed in contact with the dispersion until saturation (ca. 10 min). On average, ca. 10 cm^3 of the dispersion were introduced in the porous system of each stone block. The block was subsequently oven-dried (95 °C, 24 h). The same procedure was repeated 3 times. After 3 treatment applications the average amount of $Ca(OH)_2$ solids introduced was ca. 0.15 g per sample (ca. 0.4 wt %). Following treatment, stone blocks were placed in a plastic container and subjected to carbonation in air (as described above) for 30 days to ensure maximum conversion of $Ca(OH)_2$ into $CaCO_3$. Sandstone blocks subjected to ethanol imbibition were used as controls. Up to 4 replicates per treatment/control were performed.

Following carbonation, fresh fracture surfaces were observed with FESEM (samples were carbon coated prior to observation). In order to determine the depth distribution of calcium carbonate and its mineralogy, powder samples were collected from the treated stones at different depths using a steel saw-blade and analyzed by means of TG and XRD. Before and after treatment, color measurements (five per stone block larger surface) were done using a Minolta CM-700d spectrophotometer equipped with a pulsed Xe lamp (diffuse reflectance geometry, D65 illuminant at 10°) and using the CIELAB

dx.doi.org/10.1021/la4017728 | Langmuir 2013, 29, 11457–11470

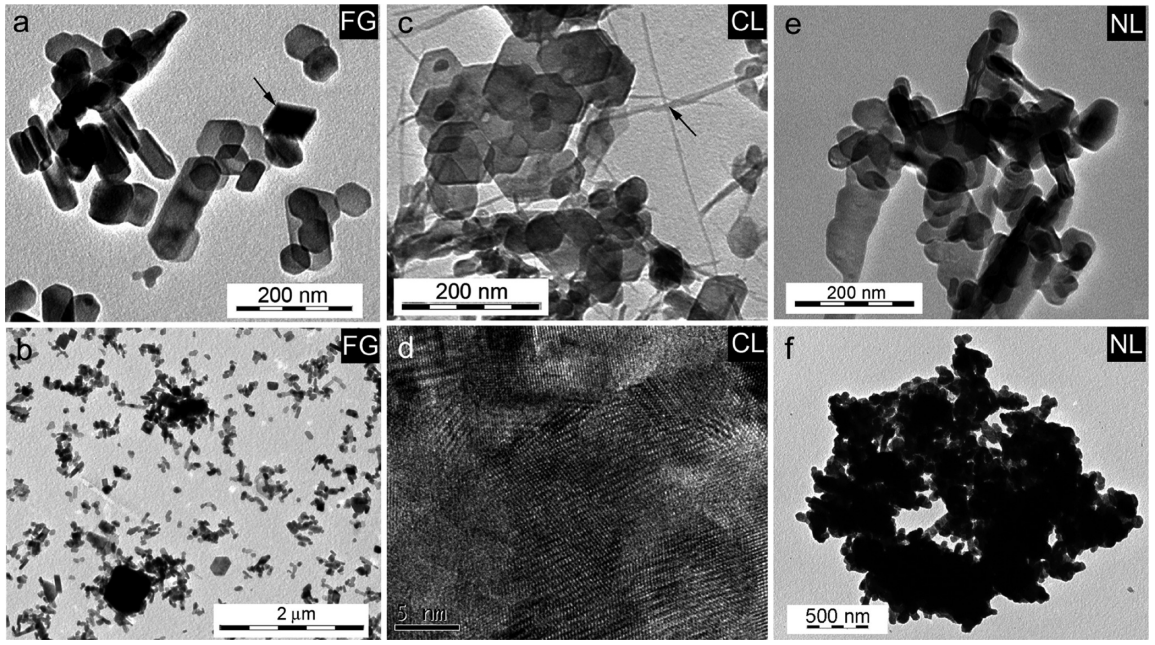

Figure 2. TEM photomicrographs of: (a) FG portlandite nanoparticles (arrow shows a calcite rhombohedrom) and (b) submicrometer- and micrometer-sized aggregates; (c) portlandite nanoporticles and zeolitic-phase fibers (arrow) in CL; (d) HRTEM image of a $Ca(OH)_2$ crystal in CL showing lattice fringes of slightly misaligned crystallites; (e) nanosized $Ca(OH)_2$ crystals in NL showing rounded edges due to beam-damage; and (f) micrometer-size aggregate of portlandite nanoparticles in NL.

color space.[29] The total color variation, ΔE, due to treatment was calculated by

$$\Delta E = \sqrt{\Delta L^{*2} + \Delta a^{*2} + \Delta b^{*2}} \quad (2)$$

where ΔL^* is the change in luminosity, and Δa^* and Δb^* are the changes in color coordinates (a^* being the red-green parameter and b^* the blue-yellow one).

A sonication test was performed to evaluate the consolidation efficacy of the conservation treatment in terms of strength gain.[30] Both control and treated (carbonated) samples were sonicated in deionized water for a duration of 5 min, five times in succession, using a 50 kHz ultrasonic bath (Ultrasons model, 200 W; J. P. Selecta). Samples were collected, dried for 24 h in an 95 °C oven, and weighed after each 5 min sonication cycle.

3. RESULTS AND DISCUSSION

3.1. Aged Slaked Lime Putty Particles (FG). XRD analysis (Figure 1a) showed that FG was made up of portlandite crystals with small amounts (<5 wt %) of calcite ($CaCO_3$). This was confirmed by TG analysis (Figure 1b) showing two main weight loss events. The first took place at 300−500 °C, and corresponded to the dehydroxylation of $Ca(OH)_2$ which was present in an amount of 94.6 wt %. The second weight loss took place at 550−800 °C and corresponded to the decomposition of $CaCO_3$ into CaO and CO_2. The amount of calcium carbonate calculated from TG was 5.4 wt %. Calcite formed due to early carbonation of the paste during sample storage and preparation (i.e., drying of the putty). Williamson-Hall plots showed that the mean crystallite size of $Ca(OH)_2$ particles was 92 ± 10 nm, with a nonuniform strain contribution to peak broadening of 0.02 ± 0.01%. The measured lattice strain is associated with the presence of crystal defects such as dislocations and/or subgrain boundaries.[24]

The FTIR spectrum (Figure 1c) showed a strong and sharp absorption band at 3641 cm^{-1} and a broad band centered at 3490 cm^{-1} corresponding to the OH stretching modes, as well as a small well-defined band at 1655 cm^{-1} corresponding to the OH bending. All of these bands are characteristic of portlandite.[31] The small sharp peak at 879 cm^{-1} and the broad band centered at 1480 cm^{-1} corresponded to the ν_2 symmetric deformation and ν_3 asymmetric stretching of CO_3 groups, respectively.[32] The latter observations confirm the presence of $CaCO_3$. The doublet at 2500−2530 cm^{-1} corresponded to atmospheric CO_2. This band could not always be successfully eliminated during the background subtraction performed prior to analysis. Raman spectroscopy also showed that FG was composed of crystalline $Ca(OH)_2$ as demonstrated by the very strong characteristic OH stretching band at 3620 cm^{-1}, as well as by the sharp band at 359 cm^{-1} corresponding to Ca−O lattice vibration (Figure 1d).[33] Additional sharp bands were observed at 157 cm^{-1} and 281 cm^{-1}, corresponding to calcite lattice modes, and at 713 cm^{-1} and 1084 cm^{-1}, associated with the υ_4 and υ_1 modes of CO_3 in calcite, respectively.[34]

N_2 sorption measurements showed that the average surface area of oven-dried FG putty was 8 ± 2 m^2/g (BET method). Its cumulative pore volume was 0.02 ± 0.002 cm^3/g. FG displayed a type II isotherm (Figure 1e), typical of mesoporous solids, with a H3-type hysteresis loop corresponding to slit-shaped pores. These are standard N_2 sorption features of slaked lime particles.[18] PSD analyses showed a polymodal particle (aggregate) size distribution with maxima at 200 nm, 700 nm, and 8.7 μm (Figure 1f). Primary $Ca(OH)_2$ crystals showed a predominantly plate-like hexagonal morphology with size (max. length) ranging from 30 to 400 nm and mean size of ∼100 nm (thickness ca. 20 nm) as revealed by TEM (Figure 2a). This mean particle size is in good agreement with crystallite size determined by XRD. Primary crystals tended to appear as aggregates with size ranging from 200 nm up to 1.5 μm (Figure 2b). These TEM observations are in good agreement with PSD results. Further details on the microstructural features of this lime putty and its rheological behavior have been reported elsewhere.[19]

dx.doi.org/10.1021/la4017728 | Langmuir 2013, 29, 11457−11470

3.2. Carbide Lime Putty Particles (CL). XRD analysis of CL particles (Figure 1a) showed the presence of broad (and weak) portlandite Bragg peaks and trace amounts of calcite (<5 wt %). As in the case of FG, the presence of calcite is due to early carbonation of the CL paste. TG analysis (Figure 1b) confirmed the presence of both $Ca(OH)_2$ (75 wt %) and $CaCO_3$ (12 wt %). In addition to these phases, the XRD analysis showed the presence of minor amounts of a calcium aluminum silicate hydrate zeolitic phase ($CaAl_2Si_7O_{18}\cdot 1.7H_2O$; JCPDS card 21−132) and a calcium aluminum hydroxide chloride hydrate phase ($Ca_2Al(OH)_6Cl\cdot 2H_2O$; JCPDS card 35−105). These phases most probably formed by reaction of $Ca(OH)_2$ with silica and alumina residua (ashes from the carbon used in the synthesis of calcium carbide). Their dehydration contributed to the small weight loss at T < 300 °C observed in TG analysis. A very weak Bragg reflection was observed at 3.3 Å which corresponded to graphite. This is a trace phase commonly present in carbide lime and responsible for its light-gray color.[21] Williamson-Hall plots showed that the average crystallite size of portlandite in CL was 34 ± 6 nm, a value nearly three times smaller than that of FG particles. The strain contribution to peak broadening was 0.15 ± 0.07%, a value nearly 1 order of magnitude higher than that of FG particles. This shows that $Ca(OH)_2$ crystals in CL paste have a higher density of defects.[25]

As in the case of FG, the FTIR spectrum of CL showed the characteristic bands of $Ca(OH)_2$ and $CaCO_3$ (Figure 1c). Interestingly, in addition to the small sharp peak at 879 cm^{-1} corresponding to the ν_2 asymmetric deformation of CO_3 groups, the ν_3 asymmetric stretching centered at 1480 cm^{-1} was broader than in FG, and was split into two peaks. These are typical features of amorphous calcium carbonate (ACC).[35] These results indicate that, in addition to ca. 5 wt % calcite detected by XRD, a fraction of the 12 wt % $CaCO_3$ in the carbide lime putty (TG results) is amorphous (i.e., undetectable to XRD). Along with hydrated calcium aluminosilicate and hydrated calcium aluminum hydroxide phases, ACC also seems to contribute to the weight loss in the range 150−300 °C observed in TG analyses. It has been reported that dehydration of ACC ($CaCO_3\cdot n$H2O, with n typically equal to 1.5) occurs in the region 90 °C < T < 257 °C.[35] The formation of ACC during carbonation of $Ca(OH)_2$ is a common phenomenom.[36] However, ACC is known for its instability: in the presence of water it readily transforms into either vaterite and/or calcite.[37] Its presence in CL appears to be associated with kinetic stabilization by organics,[38] which were added to this lime putty (lignosulfonate). The Raman spectrum of CL showed the characteristic sharp peaks at 3620 cm^{-1} and 360 cm^{-1} corresponding to the OH stretching and bending modes in portlandite, respectively. In addition, broad bands corresponding to $CaCO_3$ were observed at lower wavenumbers. In particular, the bands corresponding to lattice modes and ν_1 and ν_4 modes were very broad and shifted to lower wavenumbers (Figure 1d). These are standard Raman features of ACC.[34]

N_2 adsorption showed that the surface area of CL was 38 ± 2 m^2/g, a value consistent with the nanometric size and plate-like shape of portlandite particles in CL (see TEM results below). The features of the sorption isotherm of CL particles (Figure 1e) were similar to those of FG particles. However, the total adsorbed volume and the total pore volume (0.17 ± 0.01 cm^3/g) were 1 order of magnitude higher, and the hysteresis loop was better defined than in FG. PSD analysis showed that CL particles (aggregates) were polydisperse, with maxima at 200 nm and 11 μm (Figure 1f). TEM enabled the observation of hexagonal plate-like portlandite crystals with size ranging from 30 to 200 nm (Figure 2c), and mean particle size (number average) of 50 nm. In addition to portlandite, submicrometer-sized fibers including calcium, aluminum, and, in some cases, silicon (composition determined by EDS microanalysis) were also observed (Figure 2c, indicated by an arrow). Such fibers correspond to the zeolitic and Ca−Al hydroxide phases detected by XRD analysis. Also, some spherical shaped particles ca. 30−40 nm in size were observed, which were amorphous (SAED results, data not shown). Their size, morphology, and amorphous nature confirm that this phase is ACC.[36] As in the case of FG, primary portlandite nanoparticles tended to form aggregates with size ranging from 200 nm up to a few μm. High resolution TEM (HRTEM) showed the systematic presence of several crystallites within single $Ca(OH)_2$ crystals (Figure 2d). The lattice fringes of each crystallite were slightly misaligned, most probably due to nonperfect oriented attachment. This mosaic microstructure was more marked in this carbide lime than in typical slaked lime putty.[18] Rodriguez-Navarro et al.[18] show that one possible route for the growth of nanosized primary particles of $Ca(OH)_2$ involves the oriented attachment of crystallites a few nanometers in size. Their nonperfect oriented attachment creates defects. The presence of these defects explains the high strain contribution to XRD peak broadening in CL particles. Such defects, along with the high surface area of portlandite particles, may help to explain the high reactivity of CL (see carbonation tests below).

3.3. Commercial Nanolime Particles (NL). The fact that this sample was supplied as a 2-propanol dispersion precluded the analysis of $Ca(OH)_2$ particles dispersed in water (and dried afterward) as in the case of CL and FG. Here we report the results of the analysis of the solids obtained after oven-drying of the alcohol dispersion. XRD analysis (Figure 1a) showed that NL included portlandite (with broad and weak Bragg peaks) as the main phase, with small amounts (<5 wt %) of calcite and trace amounts of aragonite. Formation of calcite along with aragonite and/or vaterite upon (partial) carbonation of commercial nanolimes has been reported.[39] The possible formation of aragonite induced by the high T (95 °C) experienced during oven drying is ruled out because samples prepared following drying at room T under flowing N_2 also showed trace amounts of aragonite. NL had a D_{hkl} value of 55 ± 4 nm, which falls midway between those of FG and CL particles. The strain contribution to peak broadening was 0.03%. The homogeneous phase synthesis at a mild T explains the reduced lattice strain. TG analysis (Figure 1b) showed that the (apparent) amount of calcium carbonate in this nanolime was 75 wt %. As in the case of FG and CL, the formation of small amounts of calcium carbonate can be due to early carbonation during handling and sample preparation (drying). However, the high $CaCO_3$ content determined by TG is not consistent with the amount determined by XRD. The relatively small weight loss in the T range 300−500 °C, corresponding to portlandite dehydroxylation, which implies that this sample only has a 8.2 wt % $Ca(OH)_2$, plus the 6% weight loss at T below 300 °C, suggest the formation of a secondary phase upon reaction of $Ca(OH)_2$ particles with the alcohol (see also FTIR and Raman results below). The overall features of the TG trace are in very good agreement with those observed upon thermal decomposition of calcium alkoxides.[40,41] Calcium alkoxides transform into $CaCO_3$ during thermal decomposition both in air[41] and in inert (N_2) atmosphere.[40] We performed additional

dx.doi.org/10.1021/la4017728 | Langmuir 2013, 29, 11457−11470

TG analyses using N_2 atmosphere and obtained identical results to those obtained in air atmosphere. We also analyzed evolved gases with online FTIR and observed the release of alcohol and methane, in addition to CO_2, CO, and H_2O, in the T range 100−500 °C. Overall, these results show that a significant fraction of $Ca(OH)_2$ was transformed into calcium isopropoxide.

The FTIR analysis of NL showed the same features identified in FG and CL samples corresponding to calcium hydroxide and calcium carbonate. In addition, we observed a well-defined triplet at 2830−2960 cm^{-1} corresponding to the C−H stretching mode of CH_3 and CH_2, as well as the C−O (primary alcohol) stretching at 1050 and 1075 cm^{-1} (Figure 1c). These bands are characteristic of alcohols, as well as alkoxides.[41] It should be mentioned that the sample used for FTIR analysis was a powder subjected to oven-drying for 72 h at 95 °C. Thus, the observed absorption bands should not correspond to physisorbed 2-propanol. In agreement with TG results, these adsorption bands must correspond to a newly formed calcium alkoxide. Note that FTIR analyses of suspensions dried at room T under flowing N_2 also showed the same spectral features, thus confirming that alkoxide formation is not an artifact of oven drying. Although this has been neglected, it should be noted that published FTIR spectra of homogeneous phase synthesis nanolimes dispersed in 2-propanol systematically show the C−H stretching bands at 2980−2800 cm^{-1} (e.g., Figure 1b in ref 16) corresponding to a calcium alkoxide phase. Micro-Raman analysis results were fully consistent with FTIR results. In addition to the characteristic sharp peak at 3655 cm^{-1} associated with OH groups in portlandite, and the different bands of both portlandite and calcium carbonate (calcite) present at lower wavenumbers (Figure 1d), an intense broad triplet was detected at 2800−2980 cm^{-1} corresponding to the C−H stretching mode of CH_3 and CH_2 (inset in Figure 1d). These absorption bands confirm the presence of a calcium alkoxide phase.

Alkoxides are common compounds with the general formula $M(OR)_x$, where M is a metal cation of valency x and R is an alkyl or aryl group.[42] They are formed by the replacement of the hydroxylic hydrogen of an alcohol (ROH) by a metal cation. One standard route to prepare metal alkoxides is the reaction of a metal hydroxide with an alcohol:[42]

$$M(OH)_x + xROH \rightleftarrows M(OR)_x + xH_2O \quad (3)$$

This reaction is reversible, so it is necessary to remove water from the reaction system in order to have a high yield of product alkoxide. In the presence of water, the alkoxide readily transforms into the hydroxide, releasing the alcohol. It could be argued that reaction 3 readily takes place upon contact of $Ca(OH)_2$ particles with short-chain alcohols such as methanol, ethanol, and/or n-propanol. Physisorption,[43] but most commonly chemisorption, of aliphatic alcohols on portlandite crystals has been reported.[44] Day shows that $Ca(OH)_2$ powders react with methanol and suggests the possible formation of a methoxide leading to the decomposition at T ca. 700 °C of what the author called a carbonate-like product.[45] Interestingly, the results of Day's thermal analysis are very similar to those of the commercial nanolime shown in Figure 1b. Beaudoin shows that $Ca(OH)_2$ powders dispersed in methanol resulted in the formation of a calcium methoxide ($Ca(OCH_3)_2$) reaction product after 24 h.[46] Beaudoin et al. also show that other aliphatic alcohols such as 2-propanol react chemically with calcium hydroxide particles.[47] Zhang and Scherer report that cement paste, which typically contains up to 26 wt % $Ca(OH)_2$, shows an extra weight loss at T > 600 °C when treated with ethanol (solvent exchange treatment).[44] This weight loss is consistent with the formation of a reaction byproduct, whose nature was not identified by the authors. It could be argued that such a reaction byproduct is a calcium ethoxide such as $Ca(OCH_2CH_3)_2$,[41] or more generally, $Ca(OCH_2CH_3)_2 \cdot n(CH_3CH_2OH)$, with n = 2, 4.[48] The thermal decomposition of such an alkoxide produces $CaCO_3$, which in turn decomposes into CaO + CO_2 at T > 600 °C. The previous studies show that the formation of a calcium alkoxide upon contact of the commercial nanolime $Ca(OH)_2$ particles with the alcohol (2-propanol) used as dispersing medium is not only possible, but readily achievable. However, XRD patterns of the nanolime particles did not show any extra peaks that could correspond to a crystalline calcium isopropoxide. It seems that the newly formed alkoxide is poorly crystalline or amorphous and thus undetectable by XRD.

N_2 adsorption showed that NL had a specific surface area of 20 ± 1 m^2/g and a total pore volume of 0.05 ± 0.005 cm^3/g. Its sorption isotherm (Figure 1e) had the same features of FG and CL particles. PSD analyses show that $Ca(OH)_2$ particles (aggregates) are polydisperse with two relative maxima at 180 nm and 1.25 μm (Figure 1f). TEM observations showed that NL was made up of hexagonal plates of portlandite with size ranging from 20 up to 200 nm, and a mean particle size (number average) of 40 nm (Figure 2e), a value in good agreement with crystallite size determined by XRD. In agreement with laser scattering results, TEM showed that primary particles tended to form aggregates with size ranging from 200 nm up to 2 μm (Figure 2f). Unlike the case of portlandite particles in FG and CL lime putties, particles in NL were highly unstable under the electron beam, rapidly undergoing edge rounding and amorphization. This feature is consistent with the decomposition by beam damage of a thermally unstable surface precipitate a few nanometers thick, corresponding to the alkoxide identified by TG, FTIR, and micro-Raman analyses. Interestingly, the formation of such an alkoxide is pseudomorphic, that is, such a process preserves the original hexagonal morphology of portlandite crystals. This suggests that the formation of calcium alkoxides most likely occurs via a tightly coupled dissolution/precipitation replacement mechanism.[49] Such a replacement process is facilitated by a close structural similarity between reactant and product phases, which enables a topotactic (or epitactic) relationship. In the case of portlandite and calcium alkoxides, such a structural relationship exists as all these phases share a common CdI_2-type structure.[50]

3.4. Colloidal Stability of $Ca(OH)_2$ Dispersions. Figure 3 shows the absorbance (at 600 nm) of FG and CL dispersions in water, ethanol, and 2-propanol vs time. Both types of $Ca(OH)_2$ particles tended to settle rapidly when dispersed in water, thus resulting in a sudden drop in absorbance during the first minutes of the test. In contrast, a high colloidal stability was observed following dispersion of FG and CL particles in ethanol. In this case the absorbance was nearly constant throughout the whole duration of the test. Mixed results were obtained when 2-propanol was used. The colloidal stability of FG was nearly identical to that observed with ethanol, while a rapid drop in absorbance was observed in the case of CL, reaching a value similar to that of water dispersions after 2 h test-time. Note that the 2 h time-span of the test is considered enough to ensure stability during practical treatment

dx.doi.org/10.1021/la4017728 | Langmuir 2013, 29, 11457−11470

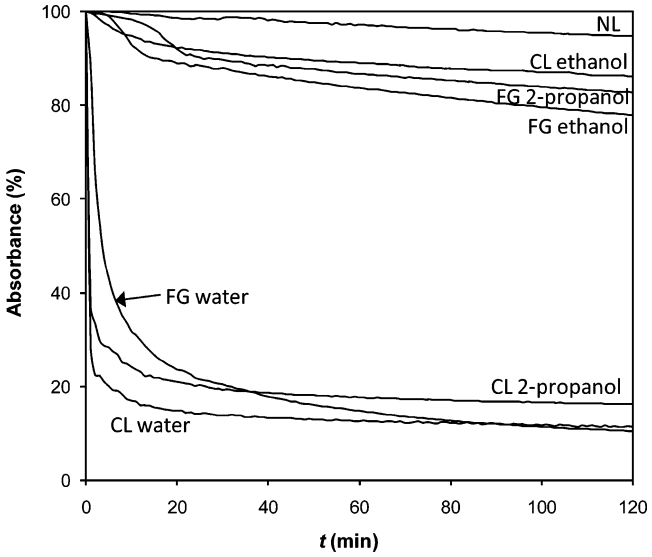

Figure 3. Colloidal stability of nanoparticle dispersions in terms of the variation of absorbance at 600 nm vs time.

application.[2] Because a high colloidal stability is critical to prevent the formation of undesired surface white glazing,[5] ethanol dispersions were thus selected for the treatment of the sandstone with both types of lime putties. In the case of NL, we used the dispersion as provided by the manufacturer. Such a 2-propanol dispersion showed a high kinetic stability, even slightly higher than that of ethanol and 2-propanol dispersions of FG and CL particles (Figure 3).

It has been shown that short-chain alcohols are highly effective in increasing the colloidal stability of $Ca(OH)_2$ nanoparticles, which otherwise aggregate and settle rapidly when dispersed in water.[5,9,11] Electrokinetic measurements show that $Ca(OH)_2$ particles dispersed in water have a zeta-potential of +34 mV,[19] while in ethanol and 2-propanol the zeta potential reportedly drops to +16.7 and +4.6 mV, respectively.[51] The low dielectric constant of these alcohols results in very small Debye lengths and reduced screening, if compared with water. This means that particles dispersed in ethanol will tend to aggregate due to attractive van der Waals forces, this effect being more pronounced in the case of 2-propanol. However, this is not what our experimental results show. Electrostatic interactions do not thus account for the increased kinetic stability of $Ca(OH)_2$ dispersions in short-chain alcohols. Detailed analyses using small-angle neutron scattering (SANS) and small-angle X-ray scattering (SAXS) show that adsorption of aliphatic alcohol molecules (2-propanol) onto $Ca(OH)_2$ particles (prepared by homogeneous synthesis) leads to kinetic stabilization, most probably due to hydrophobic (steric) interactions.[43] In contrast, particles agglomerate forming dense fractal structures when dispersed in ethylene glycol. Face-to-face aggregation of $Ca(OH)_2$ particles most probably occurs due to the presence of two opposite OH groups in ethylene glycol (i.e., it acts as a molecular bridge). Competitive adsorption in 2-propanol/ethylene glycol mixtures leads to either stabilization or aggregation, depending on the volume fraction of each solvent. In the case of CL, a competition for adsorption sites between adsorbed organics (i.e., lignosulfonate molecules) and the alcohol molecules in the solvent also seems to be at work. Apparently, 2-propanol is not able to compete for adsorption sites on the surface of $Ca(OH)_2$ as effectively as ethanol. Ultimately, the higher capacity of ethanol to effectively compete for adsorption sites leads to the higher kinetic stability of ethanol dispersions of CL particles if compared to 2-propanol ones as shown in Figure 3. This is most probably due to the favorable chain length and configuration of ethanol molecules. The absence of organics in FG lime putty leads to an effective kinetic stabilization with both ethanol and 2-propanol. In the case of NL, the absence of organic additives enables 2-propanol to provide an optimal kinetic stability associated with hydrophobic (steric) interactions.

3.5. Carbonation of $Ca(OH)_2$ Particles. XRD showed the formation of vaterite and calcite in both FG and CL dispersions, irrespective of the use of ethanol or 2-propanol as dispersing medium (Figure 4). Vaterite and calcite also

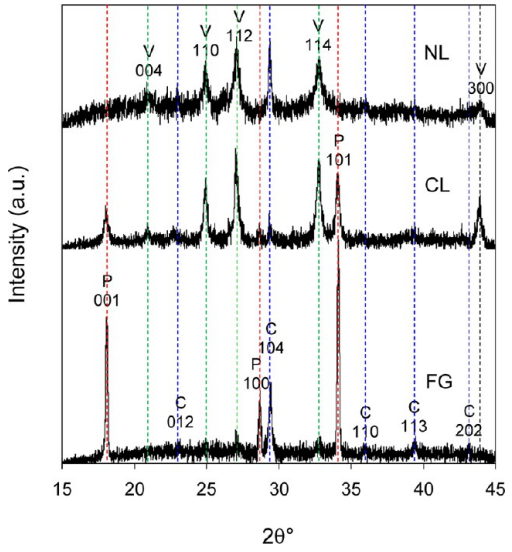

Figure 4. XRD patterns of nanolime dispersions deposited on glass slides and carbonated in air for 28 days. Main Bragg peaks for portlandite (P), calcite (C), and vaterite (V) are indicated.

formed during carbonation of the commercial nanoline (Figure 4). Calcite was the main phase throughout the whole carbonation of FG alcohol dispersions (X_C = 0.63 up to 1). Conversely, vaterite was the most abundant phase in carbonated CL alcohol dispersions, with values of X_V ranging from 0.93 after 3 days carbonation, up to 0.97 after 2 weeks air exposure. Carbonation of the NL 2-propanol dispersion resulted in the formation of vaterite (X_V up to 0.82) with minor amounts of calcite. Carbonation of FG aqueous dispersions only produced calcite, while some vaterite (X_V up to 0.24) was detected in carbonated CL aqueous dispersions. Additional carbonation tests using aqueous dispersions of lignosulfonate-free CL showed the formation of calcite without vaterite. Interestingly, carbonation of additive-free CL particles dispersed in alcohol resulted in the formation of vaterite with X_V up to 0.22 (X_C = 0.78).

These results show that, in the case of CL, the organic additive (lignosulfonate) strongly contributes to the formation of vaterite, because in its absence no vaterite formed after carbonation of CL aqueous dispersions. It has been thoroughly reported that a large number of organic molecules in solution tend to favor the formation and kinetic stabilization of vaterite, preventing/delaying its transformation into stable calcite.[52] On the other hand, the fact that only calcite forms after carbonation of FG aqueous dispersions, or CL aqueous dispersions without

dx.doi.org/10.1021/la4017728 | Langmuir 2013, 29, 11457−11470

lignosulfonate, while vaterite systematically forms after carbonation of the alcohol dispersions, strongly suggests that the tested alcohols play a role in the formation and stabilization of metastable vaterite. We will show below that this is related to the formation of calcium alkoxides.

FTIR analyses of both FG and CL $Ca(OH)_2$ particles dispersed in ethanol and 2-propanol (Figure 5) showed small

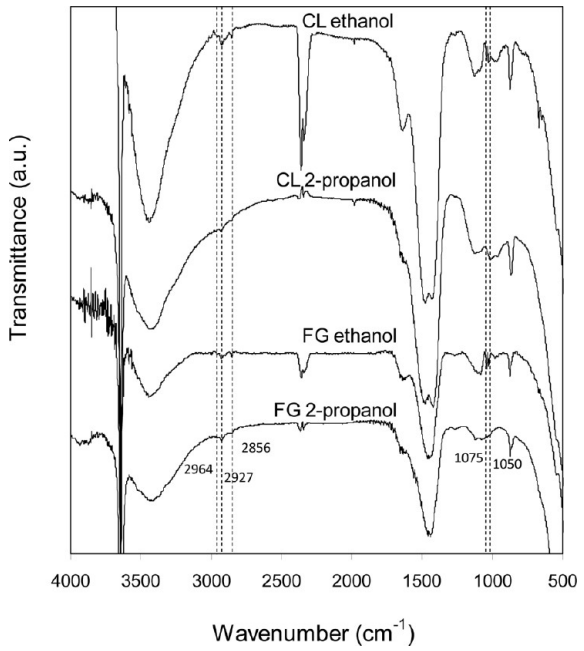

Figure 5. FTIR spectra of FG and CL $Ca(OH)_2$ nanoparticles dispersed in ethanol and 2-propanol. The vertical dotted lines show the position of bands corresponding to calcium alkoxides.

extra absorption bands at 2800−2980 cm^{-1} corresponding to the C−H stretch in CH_2 and CH_3. Also, the C−O (primary alcohol) stretching bands at 1050 and 1075 cm^{-1} were observed. These absorption bands were not present in the original FG and CL aqueous dispersions but were present in the commercial nanolime dispersed in 2-propanol (Figure 1c). As in the case of NL, the fact that the alcohol dispersions were oven-dried at 95 °C for 3 days prior to FTIR analysis, suggests that the observed extra bands correspond to a calcium alkoxide precipitate. FTIR analyses of suspensions dried at room T under flowing N_2, showed the same spectral features corresponding to an alkoxide, also confirming that its formation is not an artifact of oven drying. TG analysis of oven-dried FG alcohol (ethanol) dispersions showed an additional small weight loss at T < 300 °C (0.23 wt %) not present in the original lime putty, and an increase in the amount of $CaCO_3$ from 5.3 up to 10.7 wt %. In the case of CL alcohol (ethanol) dispersion, the additional weight loss at T < 300 °C was higher (1.29 wt %) than in FG and the amount of $CaCO_3$ decomposed at T > 600 °C increased from 11.8 up to 25.4 wt %. Online FTIR analysis of evolved gases showed the release of CH_4 and alcohol, along with CO_2, CO, and H_2O (analysis performed in N_2 atmosphere). The results of FTIR and TG-FTIR analyses are thus consistent with the formation of a calcium alkoxide precipitate in both FG and CL dispersed in alcohol. The amount of calcium alkoxide seems to be lower in FG and CL than in NL, as shown by the smaller characteristic bands and the lower increase in $CaCO_3$ detected with TG. This is probably due to the time the alcohol was in contact with the particles: in the case of FG and CL it was only two months, while the NL dispersion was purchased two years ago. Of the two lime putties dispersed in alcohol, CL showed the highest amount of alkoxide. Apparently, the amount of calcium alkoxide formed in each case depends both on the reactivity of $Ca(OH)_2$ particles, thus increasing as the particle size decreases (i.e, FG vs CL), and on the age of the dispersions (i.e., FG and CL vs NL).

In principle, the partial replacement of $Ca(OH)_2$ particles by a calcium alkoxide would not be detrimental from a consolidation point of view. Hydrolysis of calcium alkoxides to form $Ca(OH)_2$ (see reaction 3) should eventually lead to the formation of $CaCO_3$, via carbonation of the hydroxide. In fact, Favaro et al.[48] show that different calcium alkoxides can consolidate limestone via the above process. Interestingly, they report that the newly formed $CaCO_3$ cement systematically includes vaterite as the main phase. It could be argued that once the alkoxide is hydrolyzed during carbonation in the presence of humidity, the released alcohol molecules can interact with $CaCO_3$ nuclei, most probably via H-bonding, as to kinetically stabilize vaterite. It has been shown that hydroalcohol solutions (e.g., ethanol−water mixes) are highly effective in promoting the crystallization and stabilization of vaterite.[53] During carbonation of the alcohol dispersions tested here, which systematically takes places in the presence of humidity,[27] the hydrolysis of the alkoxides would release alcohol molecules forming a hydroalcoholic solution film on portlandite particles. Such a solution will favor the kinetic stabilization of newly formed vaterite, as in the cases previously reported. In addition, the formation of ACC (as observed in partially carbonated CL with lignosulfonate additive: see section 3.2) and its kinetic stabilization by the alcohol released during alkoxide hydrolysis is not ruled out. Park et al. report that ACC can be readily synthesized via carbonation of $Ca(OH)_2$ and stabilized for relatively long periods of time by different alcohols (ethanol and 2-propanol).[54] The authors report that after one week ACC transforms into vaterite with minor amounts of calcite.

The precipitation of vaterite, as well as ACC, during carbonation of nanolimes dispersed in alcohol has been reported.[23,39] The formation and stabilization of such metastable $CaCO_3$ phases may have implications on the short-term performance of a consolidation treatment as these phases are more soluble than calcite.[52] Additionally, it has been shown that differences in crystal structure between a calcitic substrate (e.g., limestone, or lime mortars and plasters) and vaterite (typically polycrystalline spherulites) would preclude the establishment of a coherent bond upon a consolidation treatment.[55] The same rationale applies to ACC. However, this short-lived phase most probably does not have any important effect on the effectiveness of the treatment. It follows that a nanolime treatment producing a minimum amount of vaterite would be preferred (e.g., FG alcohol dispersion). In the case of a noncalcitic substrate, such a shortcoming would not be that relevant. In any case, it should be noted that, due to its metastable nature, vaterite (as well as ACC) would eventually dissolve and reprecipitate as stable calcite, thus ensuring an efficient long-term consolidation. However, and unlike ACC,[38,54] the kinetics of vaterite phase transformation in air seem to be quite slow. In fact, we observed no indication for such a transformation after three months air exposure (80% RH, 20 °C).

dx.doi.org/10.1021/la4017728 | Langmuir 2013, 29, 11457−11470

Semiquantitative XRD analyses showed that both CL and NL carbonated at a faster rate than FG (Figure 6). These results are

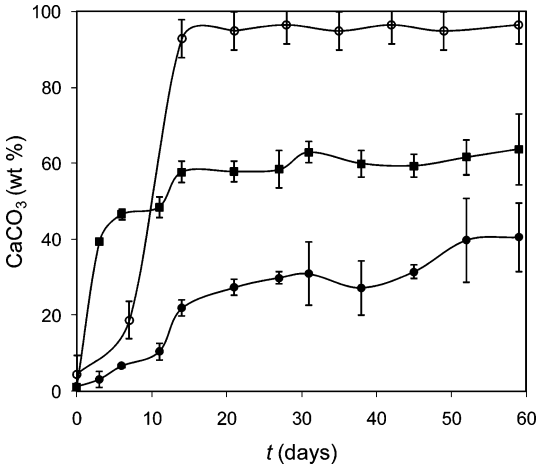

Figure 6. Degree of carbonation of FG (●), CL (■), and NL (○) alcohol dispersions deposited on glass slides vs time as determined from XRD analysis. Lines are intended as a guide to the eye.

consistent with the smaller crystal size and higher surface area (i.e., higher reactivity) of $Ca(OH)_2$ particles in CL and NL. The higher lattice strain and defect density of porlandite particles in CL (XRD and TEM results) also contribute to their higher carbonation rate. It has been shown that crystal defects increase the reactivity of solids.[56] Nonetheless, NL showed the highest carbonation rate despite the fact that its surface area was lower than that of CL by a factor of 2. Note, however, that the amount of calcium alkoxide in NL was the highest of all studied samples. Apparently, the very high reactivity of this secondary phase contributed to speeding up the carbonation of NL. From a conservation point of view, this effect could be advantageous when a fast consolidation is required. Fast carbonation kinetics are crucial for the effective short-term performance of nanolime consolidation treatments, particularly if applied as preconsolidation treatments on very friable materials.[3]

XRD results show that in all cases a full carbonation of $Ca(OH)_2$ particles deposited on glass slides is not achieved, not even after 2 months air exposure. Figure 6 shows that after an initial rapid carbonation period, the carbonation rate tends to zero after ca. 28 days. After two months, the total amount of $CaCO_3$ produced, that is, the carbonate yield,[57] reached values of 35, 67, and 95 wt % $CaCO_3$, in the case of FG, CL, and NL, respectively. Most probably, this limited yield is due to the formation of a passivating $CaCO_3$ shell on partially carbonated $Ca(OH)_2$ particles. Daniele et al.[37] report that a 100% $CaCO_3$ yield is not achieved, not even when carbonation of nanolime is performed at a high RH of 90% and for long periods of time. The authors observe a maximum $CaCO_3$ yield of 65 wt % (only calcite) after 2 month carbonation in the case of a nanolime prepared by homogeneous phase synthesis and dispersed in 2-propanol. The lower $CaCO_3$ yield and the formation of calcite observed by these authors are most probably due to the fact that they studied the carbonation of freshly made 2-propanol nanolime dispersions, where the amount of newly formed calcium alkoxide should be minimal.

A high $CaCO_3$ yield during carbonation is critical for the performance of nanolime treatments. Attempts to increase $CaCO_3$ yield include the use of additives such as $NaHCO_3$.[57] However, the formation of deleterious salts (e.g., Na_2CO_3) in the porous system of a treated material is an issue when using $NaHCO_3$. In our case, it seems that the best way to achieve a fast carbonation and a high $CaCO_3$ yield is the use of $Ca(OH)_2$ dispersions with the highest possible surface area and density of defects, such as CL. However, a higher yield and faster carbonation (after one week air exposure) is achieved when a significant fraction of $Ca(OH)_2$ has transformed into calcium alkoxide, as in the case of NL (Figure 6). The draw-back of alkoxide-enhanced carbonation is that the end-product is metastable vaterite.

3.6. Sandstone Consolidation. XRD analyses of samples collected at different depth from the sandstone treated with FG showed the presence of calcite 104 Bragg peak down to a depth of 3 mm. Conversely, only small peaks corresponding to vaterite were detected down to a depth of 3 mm in sandstone samples treated with CL and NL. In all cases no portlandite Bragg peaks could be clearly detected at any depth due to overlap with Bragg peaks of silicate phases. TG analyses, however, showed the presence of uncarbonated portlandite in concentrations of 30 wt % (70 wt % $CaCO_3$) and 15 wt % (85 wt % $CaCO_3$) in samples treated with FG and CL, respectively. The relative amount of portlandite did not change with depth. No weight loss associated to $Ca(OH)_2$ thermal decomposition was detected at any depth in stone samples treated with NL. FG and CL showed a monotonic decrease in $CaCO_3$ content with depth, while this change was not that marked in the case of NL treatment (Figure 7). The more homogeneous distribution

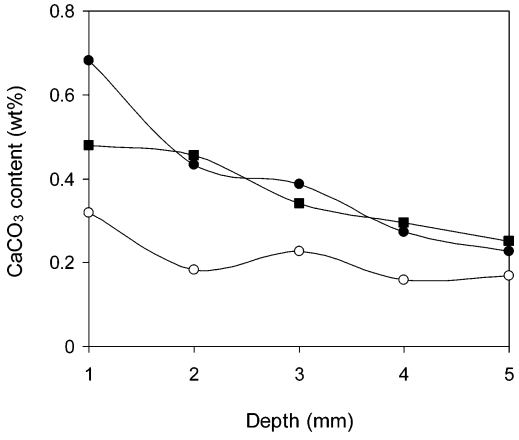

Figure 7. Total $CaCO_3$ content (wt %) vs depth in sandstone samples treated with nanolime alcohol dispersions (TG results). Symbols: ● FG; ■ CL; ○ NL. Lines are intended as a guide to the eye.

of NL throughout the pore system of the sandstone seems to be due to its smaller $Ca(OH)_2$ particle (aggregate) size. Such a homogeneous distribution led to a slightly smaller amount of $CaCO_3$ in the first few millimeters of the depth profile. TG results showing the presence of $Ca(OH)_2$ in stone samples treated with FG and CL dispersions are consistent with the limited $CaCO_3$ yield observed in carbonation tests (dispersions deposited on glass slides). However, the $CaCO_3$ yield in treated stone samples was higher than in the case of $Ca(OH)_2$ particles deposited on glass slides. Apparently, capillary condensation of H_2O in the pores of the sandstone fosters carbonation. Finally, these results show that a sufficient penetration depth was achieved in all cases, higher than that previously reported for nanolime treatments applied on bricks (<0.5 mm),[11] mural

dx.doi.org/10.1021/la4017728 | Langmuir 2013, 29, 11457−11470

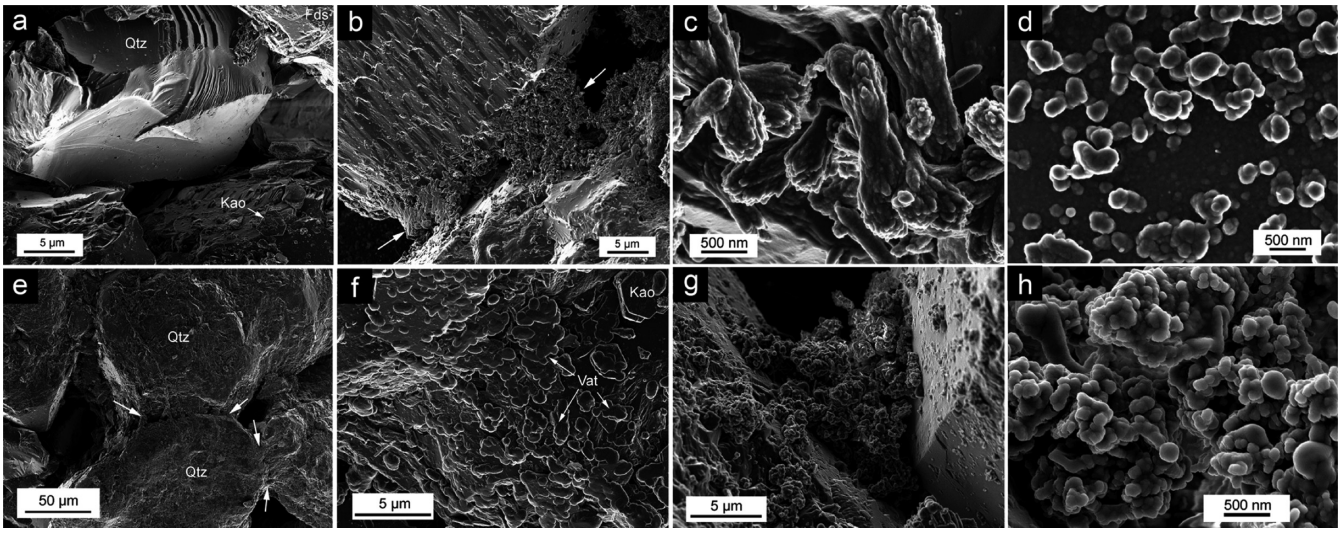

Figure 8. FESEM photomicrographs of untreated and treated sandstone: (a) control (untreated) sample showing quartz (Qtz) and feldspar (Fds) grains with sparse kaolinite (Kao) plate-like crystals; (b) newly formed $CaCO_3$ cement (arrows) deposited at the contact between silicate grains after treatment with FG; (c) detail from (b) showing the sheaf-of-wheat morphology of $CaCO_3$ (calcite); (d) detail of (scarce) spheroidal $CaCO_3$ cement (vaterite) formed on quartz after FG treatment; (e) vaterite aggregates (arrows) deposited at the contact between quartz grains following treatment with CL; (f) detail of vaterite (Vat) cement formed on a quartz grain after treatment with CL; (g) vaterite aggregates linking together quartz and feldspar grains following treatment with NL; and (h) detail of spherulitic aggregates of vaterite formed on the sandstone following treatment with NL.

paintings (200−300 μm),[13] or limestones (<100 μm up to 1 mm).[12,57] This is most likely due to the large amount of pores with size >1 μm present in the sandstone. In materials with smaller pores, such a high degree of penetration is not expected.

FESEM analyses (Figure 8) showed the presence of newly formed $CaCO_3$ cement concentrated at the contact of quartz (or feldspar) grains, linking them together without blocking or plugging the pores regardless the type of $Ca(OH)_2$ dispersion applied. The new cement concentrated at grain boundaries, where its consolidation efficiency is maximized (Figure 8b). This is most probably due to the formation of a retracting meniscus during the evaporation of the alcohol dispersion. In the case of FG, the $CaCO_3$ cement appeared as compact aggregates with a sheaf-of-wheat morphology (Figure 8c). Such a morphology is characteristic of calcite formed at a high supersaturation after ACC.[58] Minor amounts of spheroidal-shaped carbonate precipitates were also observed (Figure 8d). This morphology is typical of vaterite.[52] In contrast, the carbonate cement in sandstone samples treated with CL was systematically made up of spheroidal-shaped vaterite (Figure 8e and f). Very similar spheres and nanometer-sized aggregate of vaterite were observed cementing the sandstone following application of NL (Figure 8g and h). In this latter case, scarce calcite aggregates with a sheaf-of-wheat morphology were also observed. These observations are consistent with polymorph abundance determined by XRD analysis of carbonated $Ca(OH)_2$ alcohol dispersions.

It could be argued that the chemical and crystallographic dissimilarities between newly formed $CaCO_3$ mineral phases (i.e., vaterite and/or calcite) and quartz or K-feldspar in the silicate substrate would be a handicap for the establishment of a coherent bond, thus precluding an efficient consolidation.[55] However, sonication tests show that all treatments reduced weight loss if compared with untreated controls (Figure 9). Interestingly, the highest consolidation effectiveness was obtained after treatment with FG dispersions (35% weight loss reduction), followed by CL (22% weight loss reduction),

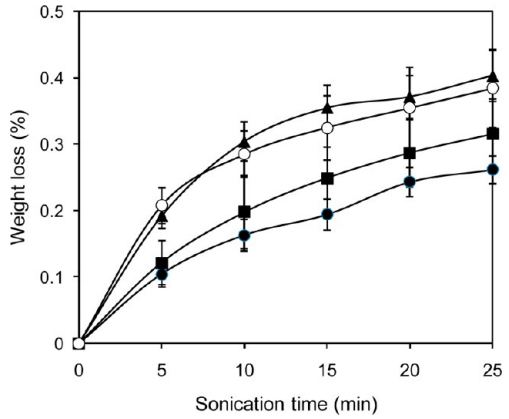

Figure 9. Weight loss vs sonication time for sandstone samples subjected to consolidation with the nanolime dispersions. Symbols: ● FG; ■ CL; ○ NL; ▲ control (untreated sandstone blocks). Lines are intended as a guide to the eye.

and finally, NL (5% weight loss reduction). The higher efficacy of FG seems to be related to the formation of calcite (with minor amounts of vaterite), as opposed to the formation of vaterite (with minor amounts of calcite) in the case of CL and NL. The significant polydispersity of aggregates in FG (and CL) could have also contributed to a higher consolidation efficiency. Chelazzi et al.[2] indicate that a mixture of nanometer and micrometer sized $Ca(OH)_2$ particles (and aggregates) could be advantageous for the effective consolidation of materials with micrometer-sized pores, as in the case of the sandstone tested here.

Despite the fact that vaterite seems to be a less effective consolidant than calcite, sonication test results, along with FESEM observations of the tight attachment of $CaCO_3$ cement onto and between quartz (and K-feldspar) grains, demonstrate that a strong bonding is established. Apparently both calcite and vaterite are effective for the consolidation of the sandstone.

dx.doi.org/10.1021/la4017728 | Langmuir 2013, 29, 11457−11470

This was not unexpected, though. First, calcium carbonate is a common cement in many sandstones and strongly contributes to their durability.[59] Second, it has been shown that building sandstones, as well as loose quartz sandy soils, can be efficiently consolidated by $CaCO_3$ (vaterite and/or calcite) produced by bacterial biomineralization (ref 55 and refs therein). Ultimately, the applied treatment mimics the natural or bacteriogenic carbonate cementation of sandstones or quartz sand, and effectively improves the physical−mechanical resistance of such a siliceous material.

Another effect that may have contributed to the consolidation of the sandstone following the application of nanolime dispersions is the reaction between the highly alkaline calcium hydroxide solution (pH 12.4) and SiO_2 grains. It has been reported that such a chemical reaction leads to the formation of amorphous/poorly crystalline (gel-like) calcium silicate phases which induce a chemical continuity between carbonated lime and silicate minerals.[60] It is interesting to note that one of the most common aggregates in lime mortars and plasters is siliceous sand.[20] The observed consolidation efficiency of $Ca(OH)_2$ nanoparticle dispersions applied on a porous siliceous stone may thus have strong implications in the conservation of lime mortars and plasters with silicate aggregates, or other silicate materials such as bricks.

Besides an improvement in the physical−mechanical properties of the treated material, a conservation treatment must not change its appearance. Spectrophotometric analyses showed that in fact all $Ca(OH)_2$ dispersions did not change the chromatic features of the sandstone. Irrespective of the treatment applied, ΔE values were systematically below 1.8. Note that the human eye is not able to detect chromatic variation with $\Delta E < 3$.[29] In particular, no white glazing was observed, as reflected by the absence of change in L^* parameter (average values of 71.1 ± 0.7 and 70.9 ± 0.6 before and after treatment, respectively). The absence of white glazing or any other undesired chromatic effects ensures that all tested $Ca(OH)_2$ nanoparticle dispersions meet the requirements for practical conservation interventions.

4. CONCLUSIONS

The analysis of the microstructural characteristics of $Ca(OH)_2$ particles in aged slaked lime putty (FG) and carbide lime putty (CL) shows that they are made up of plate-like primary nanoparticles which tend to aggregate into nonoriented submicrometer- to micrometer-sized clusters very similar to those present in the commercial nanolime (NL) produced by homogeneous phase synthesis. Once dispersed in short-chain alcohols (ethanol or 2-propanol), a high colloidal stability of $Ca(OH)_2$ particles is achieved. In the case of CL, the highest colloidal stability is achieved when the continuum is ethanol. Both ethanol and 2-propanol react with calcium hydroxide nanoparticles resulting in the formation of calcium alkoxides (calcium ethoxide or calcium isopropoxide). The formation of calcium alkoxides is a pseudomorphic replacement reaction as shown by the preservation of the external shape of the original hexagonal plates of $Ca(OH)_2$ particles. This replacement reaction most probably takes place via a coupled dissolution−precipitation mechanism and is facilitated by the fact that parent portlandite and product calcium alkoxides all possess a CdI_2-type structure. Calcium alkoxide yield depends on the reactivity of $Ca(OH)_2$ particles (surface area and lattice defects) and time of exposure to the alcohol. Calcium alkoxides play a critical role in the carbonation of the nanolime dispersions. Their hydrolysis in a humid environment speeds up the carbonation process, increases the $CaCO_3$ yield, and favors the formation of vaterite. The precipitation of this metastable $CaCO_3$ polymorph is promoted in both the commercial nanolime and the carbide lime where the degree of transformation into calcium alkoxides is the highest. In the case of the carbide lime, vaterite formation and its kinetic stabilization is also promoted by the presence of a lignosulfonate additive. In contrast, calcite formation is promoted upon carbonation of the aged slaked lime. This is due to the lower reactivity of these particles, which limits calcium alkoxide formation.

The three types of nanolime dispersions were applied onto a porous substrate (sandstone) to evaluate their consolidation capacity and to gauge their potential as conservation materials. A higher consolidation efficacy in terms of strength gain is achieved in the case of the ethanol dispersion of aged slaked lime, despite the fact that the carbonation is much faster and typically reaches a higher yield in the case of the carbide lime and the commercial nanolime alcohol dispersions. This is most probably due to the formation of a strong and coherent cement made up of stable calcite in the former case, as opposed to the formation of a cement made up of metastable vaterite in the latter ones.

The formation of calcium alkoxides, which has been neglected in previous studies, needs to be considered when applying nanolime treatments. Because their formation is time-dependent, freshly prepared alcohol dispersions would be preferred when a long-term consolidation is desired. However, when a fast precipitation and a high $CaCO_3$ yield are desired (e.g., preconsolidation treatment) a high conversion of $Ca(OH)_2$ into calcium alkoxide would be desirable. This can be achieved either by aging the alcohol dispersion for long periods of time (≫2 months) or by speeding the reaction (e.g., at a mild T). The results of this study also show that the use of alcohol dispersions of $Ca(OH)_2$ nanoparticles prepared with either aged slaked lime or carbide lime putties is an economic and effective conservation alternative to commercial nanolimes produced by homogeneous phase synthesis. Ultimately, we show that nanotechnology offers novel and effective strategies for conservation of the cultural heritage.

■ AUTHOR INFORMATION

Corresponding Author

*Tel: +34 958 246616; Fax: +34 958 243368; e-mail: carlosrn@ugr.es.

Notes

The authors declare no competing financial interest.

■ ACKNOWLEDGMENTS

This work has been financially supported by the Spanish government under contract CGL2012-35992 and the Junta de Andalucía Research Group RNM-179 and project P11-RNM-7550. E.R.A. acknowledges the receipt of a Ramón y Cajal grant. FESEM, TG, TEM, Raman spectroscopy, and PSD analyses were performed at the Centro de Instrumentación Científica of the Universidad de Granada. We thank K. Kudlacz for his help with Raman analysis and the calibration curves for semiquantitative XRD analysis. The personnel of the Dept. Inorganic Chemistry (Universidad de Granada) helped with FTIR and colloidal stability measurements. We thank F. Gordillo S.L. for donating FG quicklime, M.A. Bermejo (Trenzametal S.L.) for supplying the carbide lime putty, and

J. Ramos for providing the commercial nanolime dispersion. We also thank three anonymous referees for their insightful comments and suggestions.

REFERENCES

(1) Doehne, E.; Price, C. *Stone Conservation: An Overview of Current Research*, 2nd ed.; The Getty Conservation Institute: Los Angeles, 2010.
(2) Chelazzi, D.; Poggi, G.; Jaidar, Y.; Toccafondi, N.; Giorgi, R.; Baglioni, P. Hydroxide nanoparticles for cultural heritage: Consolidation and protection of wall paintings and carbonate materials. *J. Colloid Interface Sci.* **2013**, *392*, 42−49.
(3) Giorgi, R.; Baglioni, M.; Berti, D.; Baglioni, P. New methodologies for the conservation of cultural heritage: Micellar solutions, microemulsions, and hydroxide nanoparticles. *Acc. Chem. Res.* **2010**, *43*, 695−704.
(4) Hansen, E.; Doehne, E.; Fidler, J.; Larson, J.; Martin, B.; Matteini, M.; Rodriguez-Navarro, C.; Sebastián Pardo, E.; Price, C.; de Tagle, A.; Teutonico, J. M.; Weiss, N. A review of selected inorganic consolidants and protective treatments for porous calcareous materials. *Rev. Conserv.* **2003**, *4*, 13−25.
(5) Giorgi, R.; Dei, L.; Baglioni, P. A new method for consolidating wall paintings based on dispersions of lime in alcohol. *Stud. Conserv.* **2000**, *45*, 154−161.
(6) D'Armada, P.; Hirst, E. Nano-lime for consolidation of plaster and stone. *J. Architect. Conserv.* **2012**, 63−80.
(7) Taylor, S. C.; Hall, C.; Hoff, C. D.; Wilson, M. A. Partial wetting in capillary liquid absorption by limestones. *J. Colloid Interface Sci.* **2000**, *224*, 351−357.
(8) Salvadori, B.; Dei, L. Synthesis of $Ca(OH)_2$ nanoparticles from diols. *Langmuir* **2001**, *17*, 2371−2374.
(9) Ambrosi, M.; Dei, L.; Giorgi, R.; Neto, C.; Baglioni, P. Colloidal particles of $Ca(OH)_2$: properties and applications to restoration of frescoes. *Langmuir* **2001**, *17*, 4251−4255.
(10) Nanni, A.; Dei, L. $Ca(OH)_2$ Nanoparticles from W/O Microemulsions. *Langmuir* **2003**, *19*, 933−938.
(11) Ambrosi, M.; Dei, L.; Giorgi, R.; Neto, C.; Baglioni, P. Stable dispersions of $Ca(OH)_2$ in aliphatic alcohols: properties and application i cultural heritage conservation. *Prog. Colloid Polym. Sci.* **2001**, *118*, 68−72.
(12) Dei, L.; Salvadori, B. Nanotechnology in cultural heritage conservation: nanometric slaked lime saves architectonic and artistic surfaces from decay. *J. Cult. Herit.* **2006**, *7*, 110−115.
(13) Baglioni, P.; Giorgi, R.; Dei, L. Soft condensed matter for the conservation of cultural heritage. *C. R. Chimie* **2009**, *12*, 61−69.
(14) Baglioni, P.; Chelazzi, D.; Giorgi, R.; Poggi, G. Colloid and materials science for the conservation of cultural heritage: Cleaning, consolidation, and deacidification. *Langmuir* **2013**, *29*, 5110−5122.
(15) Daniele, V.; Taglieri, G. Synthesis of $Ca(OH)_2$ nanoparticles with the addition of Triton X-100. Protective treatments on natural stones: Preliminary results. *J. Cult. Herit.* **2012**, *13*, 40−46.
(16) Roy, A.; Bhattacharya, J. Synthesis of $Ca(OH)_2$ nanoparticles by wet chemical method. *Micro Nano Lett.* **2010**, *5*, 131−134.
(17) Giorgi, R.; Chelazzi, D.; Fratini, E.; Langer, S.; Niklasson, A.; Rådemar, M.; Svensson, J. E.; Baglioni, P. Nanoparticles of calcium hydroxide for wood deacidification: Decreasing the emissions of organic acid vapors in church organ environments. *J. Cultural Heritage* **2009**, *10*, 206−213.
(18) Rodriguez-Navarro, C.; Ruiz-Agudo, E.; Ortega-Huertas, M.; Hansen, E. Nanostructure and colloidal behavior of $Ca(OH)_2$: Implications in cultural heritage conservation. *Langmuir* **2005**, *21*, 10948−10957.
(19) Ruiz-Agudo, E.; Rodriguez-Navarro, C. Microstructure and rheology of lime putty. *Langmuir* **2010**, *26*, 3868−3877.
(20) Elert, K.; Rodriguez-Navarro, C.; Sebastian Pardo, E.; Hansen, E.; Cazalla, O. Lime mortars for the conservation of historic buildings. *Stud. Conserv.* **2002**, *47*, 62−75.
(21) Cardoso, F. A.; Fernandez, H. C.; Pileggi, R. G.; Concotto, M. A.; John, V. M. Carbide lime and industrial hydrated lime characterization. *Powder Technol.* **2009**, *195*, 143−149.
(22) Bermejo Sotillo, M. A.; Rodriguez-Navarro, C.; Ruiz-Agudo, E.; Elert, K. CO_2-capturing binder, production method thereof based on the selection, purification and optimization of carbide lime, and agglomerates having and environmental activity. Eur. Pat. EP2500328; presented May 4th 2010, published September 19th 2012.
(23) López-Arce, P.; Gómez-Villalba, L. S.; Martínez-Ramirez, S.; Álvarez de Buergo, M.; Fort, R. Influence of relative humidity on the carbonation of calcium hydroxide nanoparticles and the formation of calcium carbonate polymorphs. *Powder Technol.* **2011**, *205*, 263−269.
(24) Klug, H. P.; Alexander, L. E. *X-Ray Diffraction Procedures: For Polycrystalline and Amorphous Materials*, 2nd ed.; Wiley-VCH: New York, 1974.
(25) Williamson, G. K.; Hall, W. H. X-ray line broadening from filed aluminium and wolfram. *Acta Metall.* **1953**, *1*, 22−31.
(26) Martin-Ramos, J. D. *XPowder: A software package for powder X-Ray diffraction analysis*; http://www.xpowder.com, 2004.
(27) Beruto, D. T.; Botter, R. Liquid-like H_2O adsorption layers to catalyze the $Ca(OH)_2/CO_2$ solid−gas reaction and to form a non-protective solid product layer at 20°C. *J. Eur. Ceram. Soc.* **2000**, *20*, 497−503.
(28) Rao, M. S. Kinetics and mechanism of the transformation of vaterite to calcite. *Bull. Chem. Soc. Jpn.* **1973**, *46*, 1414−1417.
(29) Grossi, C. M.; Blimblecombe, P.; Esbert, R. M.; Alonso, F. J. Color changes in architectural limestones from pollution and cleaning. *Color Res. Appl.* **2007**, *32*, 320−331.
(30) Rodriguez-Navarro, C.; Rodriguez-Gallego, M.; Chekroun, B.; Gonzalez-Munoz, M. T. Conservation of ornamental stone by *Myxococcus xanthus*-induced carbonate biomineralization. *Appl. Environ. Microbiol.* **2003**, *69*, 2182−2193.
(31) Farmer, V. C. *The Infrared Spectra of Minerals*; Mineralogical Society: London, 1974.
(32) Gunasekaran, G.; Anbalagan, G.; Pandi, S. Raman and infrared spectra of carbonates of calcite structure. *J. Raman Spectrosc.* **2006**, *37*, 892−899.
(33) Martínez-Ramírez, S.; Fernández-Carrasco, L. Raman spectroscopy: Applications to cementitious systems. In *Construction and Building: Materials and Techniques*; Doly, S. G., Ed.; Nova Science Publishers: New York, 2011; pp 233−244.
(34) Wehrmeister, U.; Jacob, D. E.; Soldati, A. L.; Loges, N.; Häger, T.; Hofmeister, W. Amorphous, nanocrystalline and crystalline calcium carbonate in biological materials. *J. Raman Spectrosc.* **2011**, *42*, 926−935.
(35) Koga, N.; Yamane, Y. Thermal behaviors of amorphous calcium carbonates prepared in aqueous and ethanol media. *J. Thermal Anal. Calorimetry* **2008**, *94*, 379−387.
(36) Rodriguez-Navarro, C.; Cazalla, O.; Elert, K.; Sebastián, E. Liesegang pattern development in carbonating traditional lime mortars. *Proc. R. Soc. London, Ser. A* **2002**, *458*, 2261−2273.
(37) Rodriguez-Blanco, J. D.; Shaw, S.; Benning, L. G. The kinetics and mechanisms of amorphous calcium carbonate (ACC) crystallization to calcite, *via* vaterite. *Nanoscale* **2011**, *3*, 265−271.
(38) Gower, L. B. Biomimetic model systems for investigating the amorphous precursor pathway and its role in biomineralization. *Chem. Rev.* **2008**, *108*, 4551−4627.
(39) Gomez-Villalba, L. S.; López-Arce, P.; Alvarez de Buergo, M.; Fort, R. Structural stability of a colloidal solution of $Ca(OH)_2$ nanocrystals exposed to high relative humidity conditions. *Appl. Phys. A: Mater. Sci. Process.* **2011**, *104*, 1249−1254.
(40) Dongare, M. K.; Sihna, A. P. B. Thermal analysis of some metal alkoxides. *Themochim. Acta* **1982**, *57*, 37−45.
(41) Liu, X.; Piao, X.; Wang, Y.; Zhu, S. Calcium ethoxide as a solid base catalyst for the transesterification of soybean oil to biodiesel. *Energ. Fuel* **2008**, *22*, 1313−1317.
(42) Bradley, D.; Mehrotra, R. C.; Rothwell, I.; Singh, A. *Alkoxo and Aryloxo Derivatives of Metals*; Academic Press: London, 2001.

(43) Fratini, E.; Page, M. G.; Giorgi, R.; Cölfen, H.; Baglioni, P.; Demé, B.; Zemb, T. Competitive surface adsorption of solvent molecules and compactness of agglomeration in calcium hydroxide nanoparticles. *Langmuir* **2007**, *23*, 2330−2338.
(44) Zhang, J.; Scherer, G. W. Comparison of methods for arresting hydration of cement. *Cem. Concr. Res.* **2011**, *41*, 1024−1036.
(45) Day, R. L. Reactions between methanol and portland cement paste. *Cem. Concr. Res.* **1981**, *11*, 341−349.
(46) Beaudoin, J. J. Validity of using methanol for studying the microstructure of cement paste. *Mater. Struct.* **1987**, *20*, 27−31.
(47) Beaudoin, J. L.; Gu, P.; Marchand, J.; Tamtsia, B.; Myers, R. E.; Liu, Z. Solvent replacement studies of hydrated portland cement systems: The role of calcium hydroxide. *Adv. Cem. Based Mater.* **1998**, *8*, 56−65.
(48) Favaro, M.; Tomasin, P.; Ossola, F.; Vigato, P. A. A novel approach to conolidation of historical limestone: the calcium alkoxides. *Appl. Organometal. Chem.* **2008**, *22*, 698−704.
(49) Putnis, A. Mineral replacement reactions. *Rev. Miner. Geochem.* **2009**, *70*, 87−124.
(50) Goel, S. C.; Matchett, M. A.; Chiang, M. Y.; Buhro, W. E. A very large calcium dialkoxide molecular aggregate having a CdI2 core geometry: $Ca_9(OCH_2CH_2OMe)_{18}(HOCH_2CH_2OMe)_2$. *J. Am. Chem. Soc.* **1991**, *113*, 1844−1845.
(51) Giorgi, R.; Dei, L.; Ceccato, M.; Schettino, C. V.; Baglioni, P. Nanotechnologies for conservation of cultural heritage: paper and canvas deacidification. *Langmuir* **2002**, *18*, 8198−8203.
(52) Rodriguez-Navarro, C.; Jiménez-López, C.; Rodriguez-Navarro, A.; Gonzalez-Muñoz, M. T.; Rodriguez-Gallego, M. Bacterially mediated mineralization of vaterite. *Goechim. Cosmochim. Acta* **2007**, *71*, 1197−1213.
(53) Chen, S. F.; Yu, S. H.; Jiang, J.; Li, F.; Liu, Y. Polymorph discrimination of $CaCO_3$ mineral in and ethanol/water solution: Formation of complex vaterite superstructures and aragonite rods. *Chem. Mater.* **2006**, *18*, 115−122.
(54) Park, J. K.; Ahn, J. W.; Park, Y. S.; Han, C. Characteristic of crystal transition of amorphous calcium carbonate in H_2O, ethyl and propyl alcohol system. *Geosyst. Eng.* **2004**, *7*, 89−94.
(55) Rodriguez-Navarro, C.; Jroundi, F.; Schiro, M.; Ruiz-Agudo, E.; Gonzalez-Muñoz, M. T. Influence of substrate mineralogy on bacterial mineralization of calcium carbonate: Implications for stone conservation. *Appl. Environ. Microbiol.* **2012**, *78*, 4017−4029.
(56) Bisschop, J.; Dysthe, D. K.; Putnis, C. V.; Jamtveit, B. In situ AFM study of the dissolution and recrystallization behaviour of polished and stressed calcite surfaces. *Geochim. Cosmochim. Acta* **2006**, *70*, 1728−1738.
(57) Daniele, V.; Taglieri, G.; Quaresima, R. The nanolimes in cultural heritage conservation: characterisation and analysis of the carbonatation process. *J. Cult. Herit.* **2008**, *9*, 294−301.
(58) Tracy, S. L.; Williams, D. A.; Jennings, H. M. The growth of calcite spherulites from solution II: Kinetics of formation. *J. Cryst. Growth* **1998**, *193*, 382−388.
(59) Pettijohn, F. J.; Potter, P. E.; Siever, R. *Sand and Sandstone*; Springer: Berlin, 1973.
(60) Armelao, L.; Bassan, A.; Bertoncello, R.; Biscontin, G.; Daolio, S.; Glisenti, A. Silica glass interaction with calcium hydroxide: a surface chemistry approach. *J. Cult. Herit.* **2000**, *1*, 375−384.